Biology of Reproduction, 2019, 100(1), 101–111
doi:10.1093/biolre/ioy172
Research Article
Advance Access Publication Date: 21 August 2018

OXFORD

Research Article

A novel, noncoding-RNA-mediated, post-transcriptional mechanism of anti-Mullerian hormone regulation by the H19/let-7 axis†

Chunrong Qin[1,‡], Xi Xia[2,‡], Yanhong Fan[3,‡], Ying Jiang[4], Yong Chen[5], Na Zhang[6], Bahar Uslu[7], Joshua Johnson[8] and Amanda N. Kallen[9,*]

[1]Center for Reproductive Medicine, Affiliated Shenzhen City Maternity and Child Healthcare, Hospital of Southern Medical University, Shenzhen, China; [2]Department of Reproductive Medicine, Peking University Shenzhen Hospital, Shenzhen, Guangdong Province, P.R. China; [3]Department of Obstetrics and Gynecology, Third Hospital of Beijing University, Beijing, P.R. China; [4]Department of Obstetrics, Women's Hospital, School of Medicine, Zhejiang University, Hangzhou, Zhejiang, China; [5]Department of Human Anatomy and Histology and Embryology, School of Basic Medical Sciences, Fujian Medical University, Fuzhou, Fujian Province, PR China; [6]Department of Genetics and Developmental Biology, University of Connecticut Health Center, Farmington, Connecticut, USA; [7]Quinnipiac University, Frank H. Netter School of Medicine, North Haven, CT; [8]Division of Reproductive Sciences, Department of Obstetrics and Gynecology, University of Colorado Denver (AMC), Aurora, Colorado, USA and [9]Division of Reproductive Endocrinology and Infertility, Department of Obstetrics, Yale School of Medicine, Gynecology, and Reproductive Sciences, New Haven, Connecticut, USA

*__Correspondence:__ 333 Cedar St, PO Box 208063, New Haven, CT 06510. E-mail: amanda.kallen@yale.edu

†__Grant Support:__ The authors gratefully acknowledge funding and research support provided by the Reproductive Scientist Development Program (NIH-NICHD Project #K12HD000849-26), the Bennack-Polan Foundation Grant, the American Society for Reproductive Medicine, the NIH Loan Repayment Program, and the Milstein Medical Asian American Partnership Foundation. The University of Virginia Center for Research in Reproduction Ligand Assay and Analysis Core is supported by the Eunice Kennedy Shriver NICHD/NIH (NCTRI) grant P50-HD28934.
__Conference Presentation:__ Presented in oral format at the 2017 American Society for Reproduction annual meeting, Oct 28–31, 2017, San Antonio, TX.
‡denotes co-first authors.
Edited by Dr. T. Rajendra Kumar, PhD, University of Colorado Anschutz Medical Campus

Received 17 January 2018; Revised 23 July 2018; Accepted 27 July 2018

Abstract

In reproductive age women, the pool of primordial follicles is continuously depleted through the process of cyclic recruitment. Anti-Mullerian hormone (AMH) both inhibits the initial recruitment of primordial follicles into the growing pool and modulates the sensitivity of growing follicles to follicle stimulating hormone. Thus, AMH may be an important modulator of female infertility and ovarian reserve; however, the mechanisms regulating AMH remain unclear.

To evaluate AMH levels in the absence of H19 lncRNA, H19 knockout (H19KO) mice were evaluated for analysis of ovarian AMH gene expression, protein production, and reproductive function, including assessment of follicle numbers and litter size analysis. To further investigate regulation of AMH by the H19/let-7 axis, let-7 binding sites on AMH were predicted, and in vitro studies of

the effect of H19 knockdown/overexpression with let-7 rescue were performed. Lastly, response to superovulation was assessed via oocyte counts and estradiol measurements.
The H19KO mouse demonstrates subfertility and accelerated follicular recruitment with increased spontaneous development of secondary, preantral, and antral follicles. Ovaries of H19KO mice have decreased AMH mRNA and protein, and AMH mRNA has a functional let-7 binding site, suggesting a plausible ncRNA-mediated mechanism for AMH regulation by H19/let-7. Lastly, in the absence of H19, superovulation results in higher estradiol and more oocytes, suggesting that H19 functions to limit the number of follicles that mature, produce estradiol, and ovulate. Thus, AMH's inhibitory actions are regulated at least in part by H19, likely via let-7, marking this ncRNA pair as important regulators of the establishment and maintenance of the follicular pool.

Summary Sentence

The long noncoding RNA H19 regulates AMH via let-7.

Key words: AMH, ovarian reserve, H19, let-7, noncoding RNA, long noncoding RNA, microRNA, miRNA, lncRNA, infertility.

Introduction

Anti-Mullerian hormone (AMH) is a member of the TGFβ family of growth and differentiation factors (Cate, Mattaliano et al.). AMH was first identified as a glycoprotein, secreted by the fetal testis, that drives suppression of Mullerian ducts during male embryogenesis [1]. However, it has since become clear that AMH plays important roles in female ovarian folliculogenesis. In adult females, AMH is expressed in ovarian granulosa cells of small developing follicles and lost by the antral follicle stage. In the early menstrual cycle, a pool of early (primordial) follicles is recruited for growth. AMH is thought to play an inhibitory role in this recruitment process; the AMH null mouse (AMHKO) shows an accelerated recruitment and early depletion of the stock of ovarian follicles [2]. Final selection of a single dominant follicle also requires follicle stimulating hormone (FSH), and the loss of AMH expression in the mature, preovulatory follicle corresponds with the timing of acquisition of gonadotropin dependence.

AMH may play a role in modulating the sensitivity of the growing follicle to FSH. Durlinger et al. demonstrated that AMHKO mice grow more follicles under the influence of exogenous FSH than their wild-type (WT) counterparts. AMH also attenuates FSH-stimulated follicle growth in culture [3], and the FSH- and luteinizing hormone (LH)-driven induction of aromatase and p450scc expression is suppressed by addition of AMH to cultured human granulosa cells [4]. AMH itself is regulated by estradiol through ERα and ERβ in a receptor-specific manner, repressing AMH production via ERβ and stimulating AMH via ERα [5], and it has been postulated that the inhibitory effect of FSH on AMH in the growing follicle (where ERβ is prominent) may in fact be mediated indirectly via estradiol [5]. AMH is also regulated by oocyte-secreted factors including growth differentiation factor 9 (GDF9) and bone morphogenetic protein 15, which synergistically induce AMH expression in cultured human cumulus cells; this stimulatory effect is blunted in the presence of FSH. Inhibition of the SMAD3 pathway, which is involved in GDF9 signaling, also inhibited these effects (Convissar et al. 2017) [6]. Thus, AMH may act as a modulator of ovarian steroidogenesis as well as a "gatekeeper" for primordial follicle recruitment. However, much remains unknown about the factors that regulate recruitment and development of the ovarian follicular pool, including the regulation of AMH itself.

Over the last several years, noncoding RNAs, including microRNAs (miRNAs) and long noncoding RNAs (lncRNAs), have emerged as master regulators of growth and differentiation (for a review, see [7]) [7]. Granulosa-cell specific Dicer knockout mouse models, in which miRNA biosynthesis is disrupted in follicular granulosa cells, exhibit accelerated early follicle recruitment, increased follicular atresia, and aberrant AMH expression, suggesting a role for miRNAs in the regulation of AMH [8]. AMH may also, in turn, regulate miRNAs expression; Hayes et al. demonstrated that AMH induces miR-181a and 181b [9]. With regards to lncRNAs, the novel *lncRNA-Amhr2* appears to play a role in AMH signaling via AMH receptor gene activation [10]. However, to our knowledge, the regulation of AMH by miRNAs and/or lncRNAs remains poorly understood.

The lncRNA H19 was discovered as the first lncRNA over three decades ago [11]. H19 is a highly conserved imprinted gene, suggesting a physiologic pressure to maintain function; however, the specific function of H19 is still poorly understood. H19 is abundantly expressed in the early stages of embryogenesis; in the adult, expression is observed in skeletal muscle, heart, reproductive organs including ovary and uterus [12, 13]. This suggests that H19 is not postnatally repressed in ovary as had once been thought [12]. We recently showed that H19 acts as a molecular "sponge" for the miRNA let-7 (a well-conserved miRNA that functions as an RNA regulator and silencer of gene expression [14]); H19 binds let-7 and modulates its bioavailability [15]. We also showed that the steroidogenic acute regulatory protein (StAR), which governs the rate limiting step in steroidogenesis, is regulated at the posttranscriptional level by H19 and let-7; overexpression of H19, which sequesters let-7, also stimulates *Star* ([16] with commentary in [17]). Taken together, this work supports the theory that H19 regulates *Star* mRNA through sequestration of let-7, and more broadly, was the first to show that *Star* is regulated by ncRNAs at the posttranscriptional level. Since our previous work, additional research has demonstrated H19's broader role as a molecular sponge for other miRNAs, including miR-138, miR-200, and miR-152 [18–21] and shown that H19 can sponge these miRNAs in a context- and cell-specific manner and thus play contradictory roles in different cell types [21].

We show here that in mice with absent H19 expression, decreased ovarian AMH is observed, and that the H19 knockout mouse phenotype mirrors that of the AMH null mouse described above. Moreover, we show that AMH is a novel target of the H19/let-7 axis via a posttranscriptional regulatory mechanism, and that the follicular

phenotype of the H19KO mouse may be due, at least in part, to decreased AMH levels. These results further highlight the importance of the H19/let-7 axis in gene regulation and will contribute to our overall understanding of the regulation of AMH.

Materials and methods

Materials

The antibodies for AMH (mouse monoclonal, Santa Cruz Biotechnology, USA) and β-actin (rabbit polyclonal, Cell Signaling, USA) were purchased. Human let-7 miRNA mimic hsa-let-7b (Let-7b, AM17100/PM11050) and PremiR negative control (AM17110; miCon,) were purchased (Thermo-Fisher, USA). Primers for H19, AMH, and beta-tubulin were purchased from Real Time Primers (USA). The human H19 expression vector pH19 was previously described [16]. siH19 and siCON (n253566) were purchased from Life Technologies (Thermo-Fisher, USA).

Mouse strains and animal care

H19-delta3 knockout mice were used for this study. The $H19^{\Delta 3}$ mouse is on a C57Bl/6J background and is characterized by deletion of the 3-kb transcription unit upstream of the *H19* gene itself [22], allowing us to evaluate the effects of H19KO on folliculogenesis, steroid hormone production, and reproductive outcomes. Controls for H19KO females were WT C57Bl/6J littermates. Animals used in these studies were maintained and euthanized according to principles and procedures described in the National Institutes of Health *Guide for the Care and Use of Laboratory Animals*. These studies were approved by the Yale University Institutional Animal Care and Use Committee and conducted in accordance with the Society for the Study of Reproduction's specific guidelines and standards.

Fertility testing and determination of estrous cycles

H19KO and WT females (n = 10 per group) were housed with WT stud males of proven fertility for at least 6 months. The litter sizes were recorded continuously. Stages of the estrous cycle were determined by daily vaginal smears collected from H19KO and WT mice (n = 5 per group) between 1200 and 1500 h. All mouse estrus cycle staging was performed by a single trained laboratory member (Y. Chen) using published protocols [23]. In brief, proestrus was defined as nucleated epithelial cells with none or few leucocytes; estrus, as numerous keratinized cells with degenerate nuclei; metestrus, as abundant infiltration of leukocytes; and diestrus, as the appearance of leukocytes mixed with nucleated epithelial cells.

FSH and estradiol quantification

After retroorbital blood collection per Yale IACUC protocol at each estrus cycle stage, blood was allowed to clot and serum supernatant removed, and sent to the University of Virginia Center for Research in Reproduction Ligand Assay and Analysis Core, where FSH measurement and estradiol quantification was performed. For FSH measurement, radioimmunoassay was performed per laboratory protocol [24]. For estradiol, the Calbiotech Mouse/Rat Estradiol enzyme linked immunosorbent assay (ELISA) Kit (Calbiotech, USA) was utilized, which has a standard range of 3–300 pg/mL and a sensitivity of 3 pg/mL.

RNA-seq and data analysis

RNAs were extracted from 8-week-old WT and KO ovaries using the Purelink RNA mini kit (Cat. no. 12183018A). RNA-seq libraries were prepared using the Illumina TruSeq Stranded Total RNA LT kit with Ribo-Zero Human/Mouse/Rat, setA (Cat. no. rs-122–2201) according to the sample preparation protocol. Briefly, 1 μg of total RNA was subjected to Ribo-Zero depletion to remove rRNAs. The remaining RNA was purified, fragmented, and primed with random hexamers for cDNA synthesis. After first and second cDNA synthesis, cDNA fragments were adenylated and then ligated to indexing adapters. The cDNA fragments were enriched by PCR, purified and then sequenced on an Illumina NextSeq500 using paired-end chemistry and 76-bp cycles. Illumina BaseSpace (https://basespace.illumina.com/) embedding tools were used to analyze the RNA-seq data. RNA-Seq Alignment v1.0.0 was used to map sequencing reads to mm10 genome and quantify reads of genes. DE-Seq2 v1.0.0 was applied to calculate differential expression of genes.

Gene expression and protein quantification

Quantitative RT-PCR and western blot analyses were carried out as previously described [16]. In brief, for quantification of AMH from whole ovary, intact ovaries were removed from 8 week H19KO and WT mice (n = 5 per group) and flash-frozen for extraction of total ovarian RNA. RNA extraction was performed using the RNEasy Mini Kit (Qiagen, USA), and cDNA was synthesized using a Bio-Rad iSCRIPT kit (Bio-Rad, USA) in a 20-μl reaction containing 0.5 μg of total RNA. Quantitative PCR was performed in a 25-μl reaction containing 0.5 to 1.5 μl of cDNA using iQSYBR-Green (Bio-Rad, USA) in a Bio-Rad iCycler. PCR was performed by initial denaturation at 95°C for 5 min, followed by 40 cycles of 30 s at 95°C, 30 s at 60°C, and 30 s at 72°C. Specificity was verified by melting curve analysis and agarose gel electrophoresis. The threshold cycle values of each sample were used in the post-PCR data analysis, and the $\Delta\Delta$ threshold cycle method was used to calculate mRNA levels. The PCR primers for indicated human and mouse genes are listed; β-tubulin was used as a reference gene.

- Human H19 forward: 5′-GCACCTTGGACATCTGGAGT-3′
- Human H19 reverse: 5′-TTCTTTCCAGCCCTAGCTCA-3′
- Mouse AMH forward: 5′-GCTAGGGGAGACTGGAGAAC-3′
- Mouse AMH reverse: 5′-CCACGGTTAGCACCAAATAG-3′
- Human/mouse beta-tubulin forward: 5′-CGTGTTCGGCC AGAGTGGTGC
- Human beta-tubulin reverse: 5′-GGGTGAGGGC ATGACGCTGAA

RNA extraction and quantitative reverse transcription polymerase chain reaction (qRT-PCR) were performed in a similar fashion using cell culture lysates for analysis of gene expression in KGN cells.

To measure AMH protein levels in H19KO and WT mice, intact ovaries were removed from 8 week mice (n = 5 per group), and tissues were lysed in three volumes of 2× sodium dodecyl sulfate (SDS)-sample buffer by heating at 95°C for 5 min with occasional vortexing to break chromosomal DNA. Cell lysates (5 to 10 μl/well) were resolved on 10% SDS polyacrylamide gel electrophoresis, followed by western blot analysis using AMH primary antibody (1:500) and goat anti-mouse secondary antibody (1:2000). β-actin antibody (1:2000) was used as a control.

Bioinformatic analysis

To investigate potential regulation of AMH by the H19/let-7 axis, let-7 binding sites in the AMH gene were predicted using the web-based program RNAhybrid. RNAhybrid predicts microRNA (miRNA) targets by calculating the minimum free energy of hybridization between target RNA and miRNA sequences to predict miRNA/target duplexes [25].

Cell culture and transfection

Human KGN cells were a gift from Emre Seli, PhD (Yale University, USA). The KGN cell line is a granulosa cell line originating from a granulosa cell carcinoma (Nishi et al., 2001) [26]. All cells were cultured using standard protocols provided by the ATCC (American Type Culture Collection, USA). Cells were maintained in 100-mm culture dishes in DMEM-F12 with 10% fetal bovine serum (FBS) (heat inactivated), 1% l-glutamine, and 1% penicillin-streptomycin.

Transfections were perfomed at a 48-well plate scale. To prepare plasmid transfection solution, 0.2 μg H19 plasmid DNA per well was mixed with 25 μl OPTI-MEM (Thermo-Fisher, USA) per well by gentle pipetting. In parallel, 2 μl of lipofectamine 2000 per well was mixed with 25 μl of OPTI-MEM per well. After 5 min of incubation at room temperature, the two solutions were mixed by gentle pipetting and incubated for 20 min at room temperature to allow plasmid/lipid complexes to form. At the end of incubation, the 50 μl/well transfection solution was used to resuspend the cell pellet (5×10^5 cells/well). After incubation at room temperature for 10 min, regular growth medium was added at a ratio of 1:3, and the cell suspension was transferred to the culture plate. After 24-h incubation at 37°C in 5% CO_2, the medium was replaced with fresh growth medium. RNA and protein were extracted at the indicated time points after transfection. For H19 knockdown experiments, KGN cells were cultured at 37°C with 5% CO_2 in 24-well plates in DMEM/F12 (Invitrogen) supplemented with 10% FBS and 1% penicillin-streptomycin. We then performed *H19* siRNA KD by transfection of si*H19* or siCon using our previously described methods [15, 16]. Forty-eight hours following transfection, RNA extraction and RT-PCR were performed as described above. For let-7 mimic transfection, 1 pmol of control miRNA (miCon) or let-7b mimic was mixed with 50 μl of OPTI-MEM. In parallel, 0.5 μl of Lipofectamine 2000 was mixed with 50 μl of OPTI-MEM. After 5 min of incubation, the two solutions were mixed and incubated at room temperature for 20 min. The resulting 100 μl of transfection cocktail was added to KGN cells prewashed with OPTI-MEM. Cells were harvested at 12 h post-transfection, and AMH RNA levels were determined by qRT-PCR. Results are representative of five independent transfection experiments.

Ovarian histology and follicle counting

Fresh ovaries from H19KO and WT mice (n = 5 per group) were prepared using previously described protocols [27]. Briefly, ovaries were extracted and cleaned from the fat, rinsed in PBS, and fixed in Dietrich fixative (30% ethanol, 10% formalin v/v using aqueous 37% formaldehyde solution, 2% glacial acetic acid) overnight. Ovaries were transferred to 70% ethanol and embedded in paraffin. Five micrometer serial sections were cut and placed onto glass slides (AML Laboratories, USA), then stained with Weigert's Iron Hematoxylin, followed by picric acid counterstaining per previously published protocols [27].

After mounting, specimen coding and blinding, the total numbers of primordial, primary, and preantral follicles were counted in every tenth section. Follicles were classified as previously described by Dioguardi et al. [27] and Uslu et al. [28]. In brief, follicles were scored as primordial follicles if there was a compact oocyte surrounded by a single layer of squamous pregranulosa cells, as primary follicles if there was an enlarged oocyte surrounded by at least a single layer of cuboidal granulosa cells, and as small, preantral follicles if there was an enlarged oocyte surrounded by at least a partial or complete second layer of cuboidal granulosa cells and no more than four layers of cuboidal granulosa cells. Follicular loss/atresia was characterized by identification of oocyte remnants (showing signs of degeneration or fragmentation) or pyknotic nuclei in granulosa cells. Only follicles with an observed nucleus were scored in each section. Percentage of follicles per ovary was calculated by dividing the number of each follicle type counted by the total number of follicles counted.

Oocyte collection

H19KO and WT females (8–12 weeks old; n = 5 per group) were superovulated with 5 IU PMSG (Fisher-Scientific, USA) × 2, 24 h apart, followed 24 h later with 5 IU hCG. Ooyctes were collected from oviducts and counted 16 h post-hCG. Estradiol levels were quantified after superovulation as described above.

Statistical analysis

All data are presented as mean ± SD. Data were analyzed using two-tailed Student *t* test, with the exception of ELISA data, which was analyzed using one-way ANOVA. *P* values at 0.05 or less were considered significant. All statistical analysis was performed using GraphPad software.

Results

H19 KO female mice have decreased litter sizes and altered estrus cyclicity

In order to first quantify the effect of H19KO on fertility in vivo, we monitored litter sizes in H19KO mice and compared these to WT mice over time. We found that litter sizes were decreased in 8 week H19KO mice as compared to WT; however, the decrease in litter sizes did not reach statistical significance until after 9 months of age. (Figure 1; n = 10 mice per group). These results suggest that the aging KO female mice demonstrates impaired fertility in comparison with its WT counterpart. We also characterized estrus cyclicity and FSH and estradiol levels across the estrus cycle in H19KO mice (n = 5 mice per group) and found that total estrus cycle length was increased in H19KO mice (Figure 2a and b); differences in FSH and estradiol levels were not significant (Figure 2c and d).

AMH is decreased in ovaries of H19KO mice

So far, we have shown that the H19KO mice display phenotypes that overlap with those of AMHKO mice. To begin to delineate the underlying mechanisms linking H19 deletion to altered folliculogenesis and subfertility observed, we performed genome-wide transcriptome analysis (RNA-seq) on WT and H19KO ovaries (Supplemental Table 1; RNA sequencing data available at GEO with accession number GSE114182). Among the numerous genes whose expressions were altered by H19 deletion was AMH, which was further confirmed by RT-qPCR and western blot analyses (Figure 3, representative blot; n = 7; $P < 0.01$). These results suggest that H19 regulates AMH expression.

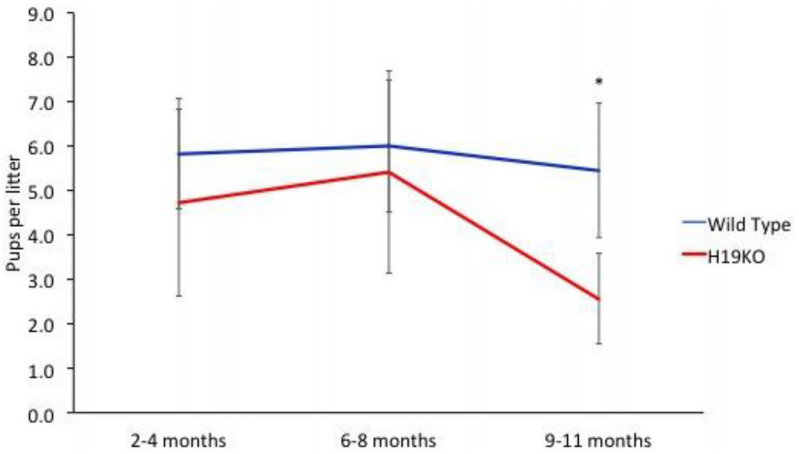

Figure 1. Litter sizes were decreased in H19KO mice. The decrease in litter size observed was not statistically significant in younger mice, but reached statistical significance at 9 months of age. N = 10 mice per group; $^{*}P < 0.05$.

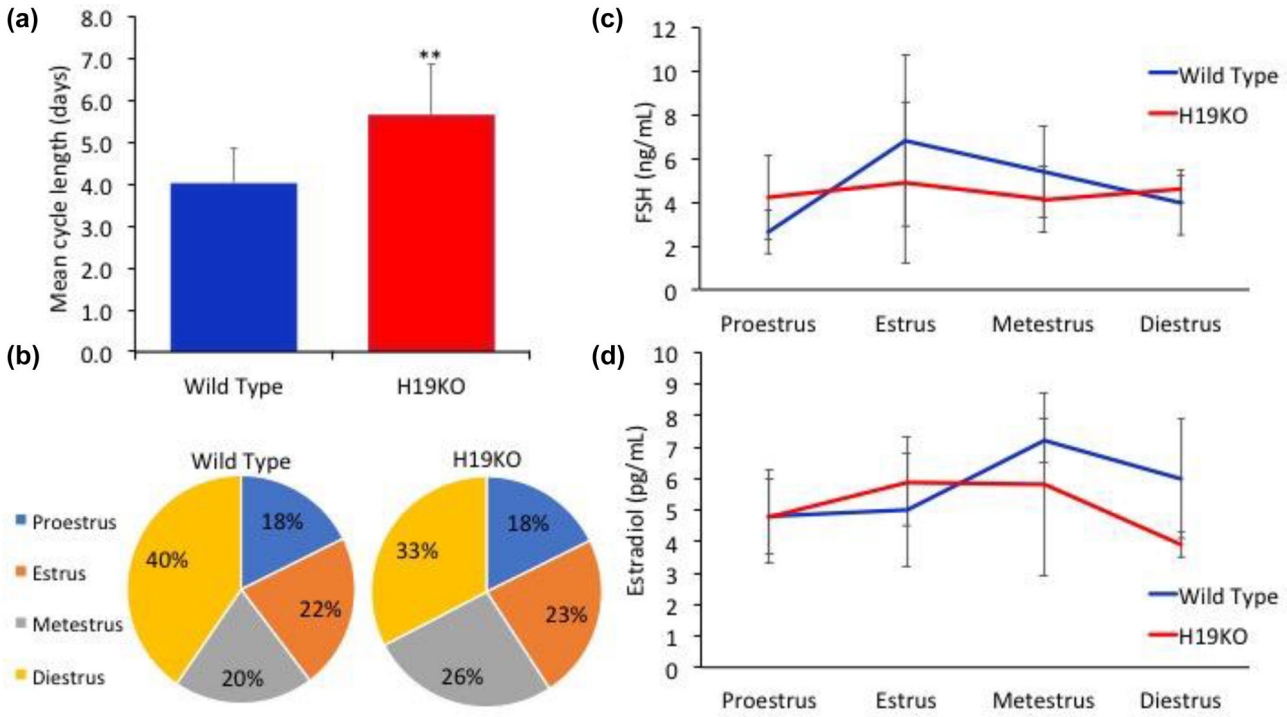

Figure 2. Estrus cyclicity, FSH, and estradiol in H19KO mice. (a) Total estrus cycle length was significantly increased in H19KO mice, (b) metestrus was prolonged in H19KO mice. (c) Differences in FSH and (d) estradiol levels (Figure 2d) were not significant. n = 5 mice per group; $^{**}P < 0.01$.

AMH is regulated by the H19/let-7 axis

Preliminary bioinformatic analysis revealed several putative let-7 binding sites in the AMH mRNA (Table 1).

KGN cells were used as a model system to test in vitro effects of altered H19 expression and let-7 rescue on AMH mRNA levels. H19 knockdown (which increases bioavailable let-7) decreases AMH mRNA by nearly half (Figure 4a and b; n = 5; $P < 0.05$) and H19 overexpression (which decreases bioavailable let-7) increased AMH mRNA by over two-fold (Figure 4c and d; n = 5; $P < 0.05$). To confirm the functionality of the predicted let-7 binding site in AMH mRNA, we tested the effect of let-7b on inhibition of endogenous AMH expression. Treatment of KGN cells with let-7 mimic led to a 60% decrease in AMH levels (Figure 5; n = 4; $P < 0.01$) demonstrating the functionality of these binding sites and supporting AMH as a target of let-7 inhibition in granulosa cells.

H19KO female mice show altered folliculogenesis and increased follicular atresia

The ovaries of 7-week-old female H19KO mice contained significantly fewer primordial and primary follicles and a larger number of secondary and preantral follicles than age-matched WT mice. Data represent the mean number of follicles per section counted (Figure 6; n = 5; $^{*}P < 0.05$; $^{**}P < 0.01$). Notably, this pattern

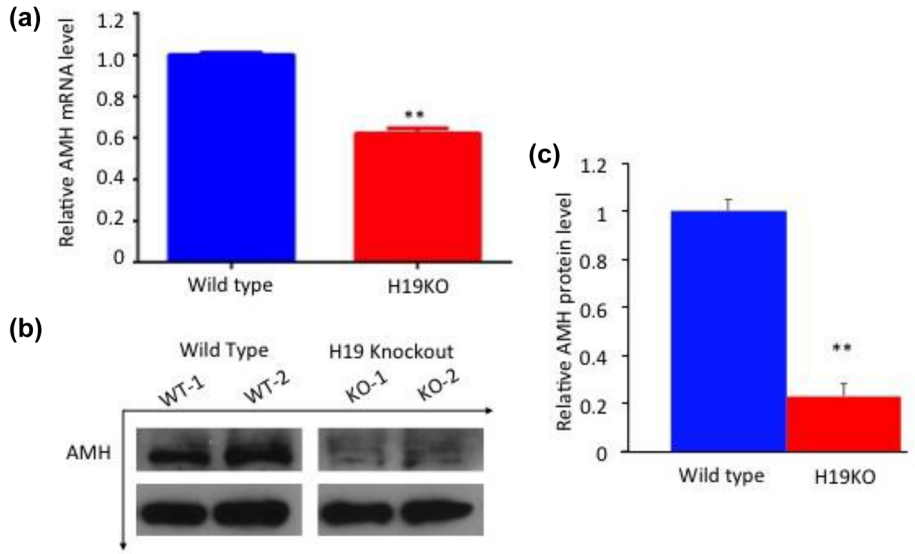

Figure 3. Decreased AMH mRNA and protein in H19 KO mice. (a) AMH mRNA expression and (b and c) protein production (representative blots, AMH antibody concentration 1:500) were decreased in whole ovaries from 8-week-old H19KO mice compared to WT mice (n = 7 ovaries per group; $^{**}P < 0.01$).

Table 1. Human AMH mRNA contains let-7 binding sites at its 3′UTR. Let-7 binding sites in the AMH gene were predicted using the web-based program RNAhybrid. Preliminary bioinformatic analysis revealed several putative let-7 binding sites in the AMH mRNA. In particular, a binding site was predicted at position 775 in the 3′UTR of human AMH mRNA. Partial sequences of AMH (in red) and let-7 are shown.

miRNA	Position	Sequence	Binding energy
Let-7b	775	5′G A UGGACACCA U3′ CACACGGCC GC UGCCUU GUGUGUUGG UG AUGGAG 3′UUG A U5′	−24.9 kcal/mol
Let-7c	769	5′C GCAC A UGGACACCA U3′ AGCCA ACGGCCGC UGCCUU UUGGU UGUUGGUG AUGGAG 3′ A A U5′	−22.8 kcal/mol
Let-7i	222	5′G UAU G C3′ AACAGC GAUAUGCCUU UUGUCG UUAUAUGGAG 3′ UGU G G U5′	−20.6 kcal/mol
Let-7j	772	5′C CGGCC GACACC U3′ CAGCACA AGCUG AUGCCUU GUCGUGU UUGAU UAUGGAG 3′UAUA U5′	−24.3 kcal/mol
Let-7j	222	5′G U U C3′ AACAGC AUGAG AUGCCUU UUGUCG UGUUU UAUGGAG 3′ UA GAU U5′	−21.7 kcal/mol
Let-7k	775	5′G AGCUGGACA A U3′ CACACGGCC CCUGCCUU GUGUGUUGG GGAUGGAG 3′ A U5′	−23.7 kcal/mol

mimics the pattern of earlier follicular recruitment and exhaustion seen in AMHKO mouse ovaries [2]. H19KO mouse ovaries also contained significantly more atretic secondary and preantral follicles (Figure 7; n = 5; $^{*}P < 0.05$; $^{**}P < 0.01$).

H19 KO female mice demonstrate an enhanced response to superovulation

Significantly, more oocytes were obtained from 8–12 week H19KO mice after controlled ovarian hyperstimulation compared to WT mice (Figure 8a; n = 7, $P < 0.05$). At time of oocyte collection, estradiol levels were higher in H19KO mice as compared to WT mice (Figure 8b; n = 5, $P < 0.01$).

Discussion

We find that the H19KO mouse demonstrates features strikingly similar to that of the AMHKO mouse, including accelerated follicular recruitment and subfertility. In the absence of H19,

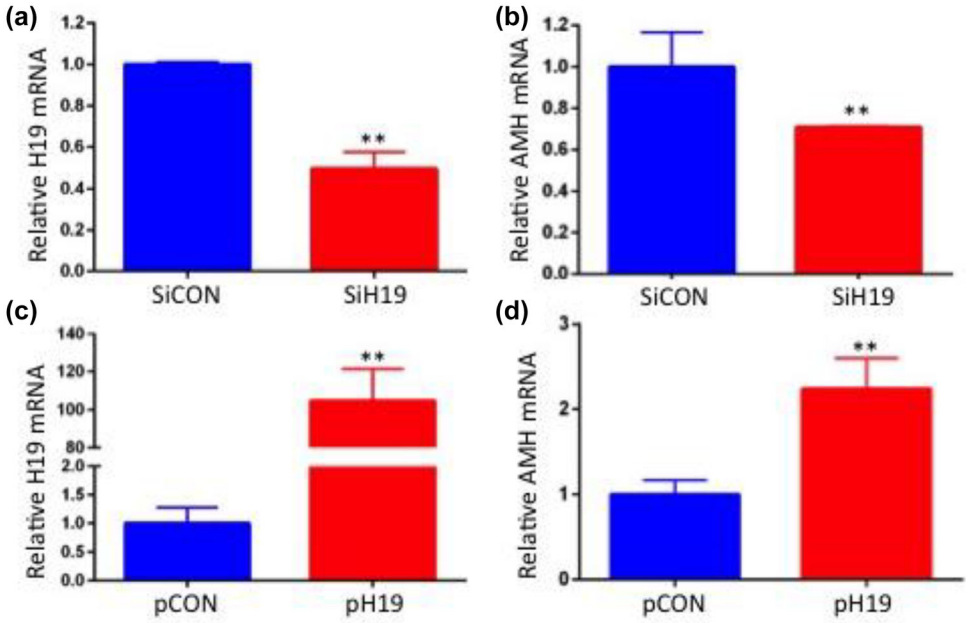

Figure 4. AMH expression decreases in response to H19 knockdown, and increases in response to H19 overexpression. (a) KGN cells were transfected with nonspecific siRNA (siCON) or siH19, as well as with (b) empty vector or pH19. RNAs were isolated 48 h post-transfection and analyzed by qPCR (n = 5; $^{**}P < 0.01$).

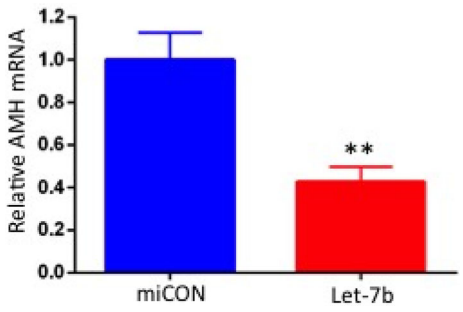

Figure 5. The predicted let-7 binding site is functional. To confirm the functionality of the predicted let-7 binding site in AMH mRNA, we tested the effect of let-7b on inhibition of endogenous AMH expression. Thus, let-7b (or miRNA negative control miCON) was transfected into KGN cells. RNA was extracted 48 h later, and AMH mRNA levels were determined by qPCR. Let-7 transfection led to decreased AMH expression, supporting AMH as a target of let-7b inhibition in granulosa cells (n = 5; $^{**}P < 0.01$).

spontaneous development of secondary, preantral, and antral follicles is significantly increased. We also observe that the ovaries of H19KO mice are characterized by decreased AMH mRNA and protein, and that AMH mRNA has a functional let-7 binding site, suggesting a plausible ncRNA mediated mechanism for AMH regulation by the H19/let-7 axis (Figure 9). Lastly, in the absence of H19, superovulation results in higher estradiol and higher oocyte production (similar again to the AMHKO mouse) as compared to WT, suggesting that H19, via AMH, may function to limit the number of follicles that mature, produce estradiol, and survive to ovulate, at least in the context of superovulation. This premature follicular recruitment at baseline, and enhanced oocyte production in the presence of high FSH levels, suggests an increased sensitivity toward FSH in H19KO mice. We previously showed that ectopically expressed H19 sequesters endogenous let-7, leading to derepression of let-7 targets [15]. Taken together, these results demonstrate that AMH is a novel target of the H19/let-7 axis, regulated via a posttranscriptional regulatory mechanism, and that the follicular phenotype of the H19KO mouse may be due, at least in part, to decreased AMH levels. These results further highlight the importance of the H19/let-7 axis in gene regulation and will contribute to our overall understanding of the regulation of AMH. H19 may act in part via AMH to serve as a brake on follicular recruitment in order to facilitate appropriate follicular growth and modulate the response to ovarian superovulation.

In reproductive age women, the pool of primordial (resting) follicles is continuously depleted via cyclic recruitment. Ongoing follicular recruitment and atresia leads to a gradual decline in follicle number until natural menopause is reached [29]. AMH is a known regulator of this process of primordial follicle recruitment [30, 31]. During the reproductive years, AMH levels correlate with the size of the primordial follicle pool [29], and AMH declines with ovarian aging, decreasing to undetectable levels until natural menopause is reached [29]. AMH thus serves as a biomarker for ovarian reserve, as well as a predictor of response to ovarian stimulation in assisted reproductive technology [31]. Immunohistochemistry of human ovarian tissue demonstrates that AMH expression is absent in primordial follicles, and highly expressed in growing follicles until the antral stage [32]. Treatment of prepubertal- and reproductive-aged mice with AMH results in significantly higher percentages of primordial and primary follicles, whereas the ovaries of AMH null mice exhibit accelerated recruitment and depletion of primordial follicles [2]. Concurrent with this finding, AMH null mice ultimately cease ovulating earlier (56% by 16–17 months) than their WT counterparts (18% by the same age) [3]. We observed a similar phenotype, included accelerated follicular recruitment, depletion of primordial follicles, and decreased litter size over time, in H19KO mice.

It has been proposed that AMH is also an important intraovarian regulator of follicular atresia [31, 29]. AMH-treated animals exhibit

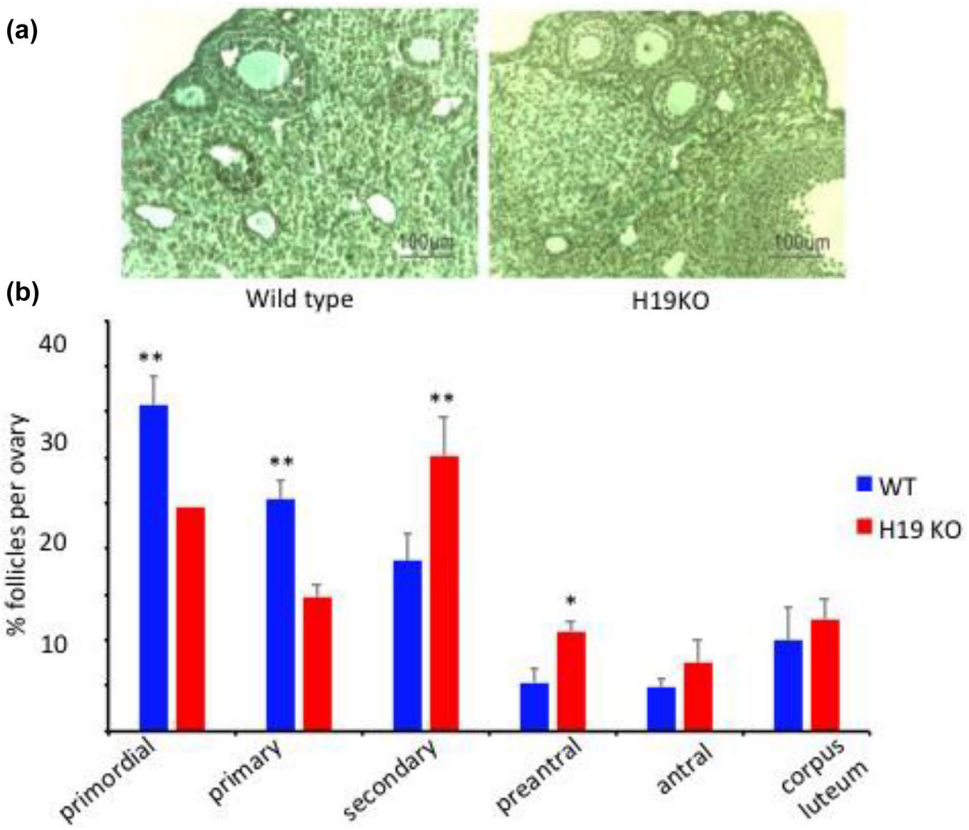

Figure 6. Follicle population in 7-week-old H19KO mice. (a) Representative section of WT and H19KO mouse ovaries. (b) Significantly fewer primordial and primary follicles, and more secondary and preantral follicles, were detected in H19KO mice as compared to WT mice. The percentage of antral follicles was nonsignificantly increased in H19KO mice, and no significant difference in the number of corpora lutea was observed. Data represent the percentage of each follicle type per ovary (n = 5 mice; $^{*}P < 0.05$; $^{**}P < 0.01$).

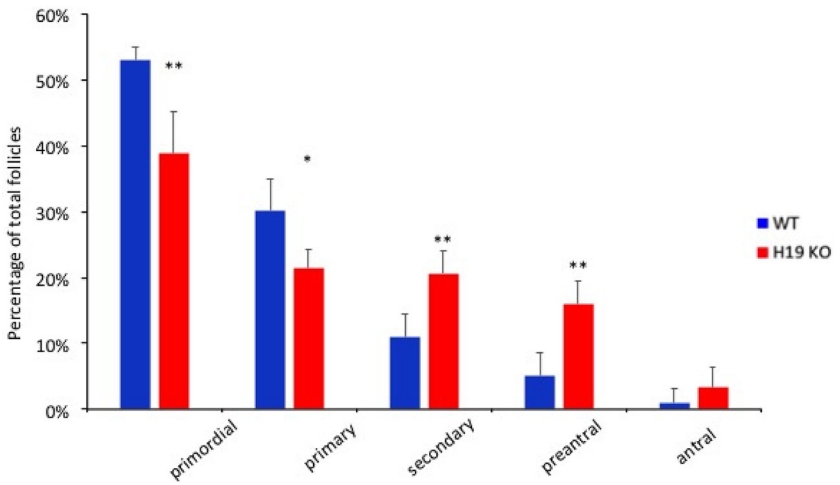

Figure 7. Atretic follicle population in 7 week H19KO mice. H19KO mouse ovaries contained significantly more atretic secondary and preantral follicles (n = 5; $^{*}P < 0.05$; $^{**}P < 0.01$).

decreased rates of follicular atresia [9]. We observed higher rates of atresia in large follicles from H19KO mice as compared to WT, similar to patterns observed in AMHKO mice. Unexpectedly, in small follicles of H19KO mice, we observed lower rates of atresia. This may be related to more efficient growth of follicles to the preovulatory stage in H19KO mice (and in fact, a similar phenomenon is observed in the AMHKO mouse, albeit in older females). As H19 expression appears to rise with increasing follicular maturity [12], it may be that the absence of H19 in small follicles plays little role in early follicular atresia. Alternatively, AMH is decreased but not absent in H19KO mice; thus, H19 may be an important regulator of AMH, but not the primary driver of AMH production. Lastly, that

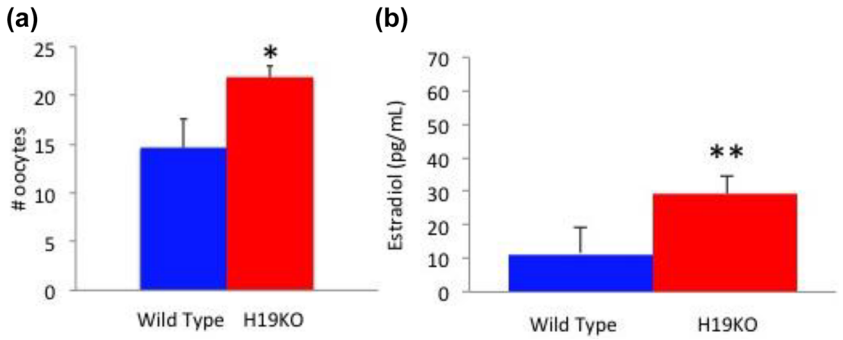

Figure 8. Oocytes produced and estradiol levels in response to superovulation in H19KO mice. (a) Significantly more oocytes were obtained from 8 to 12 week H19KO mice after controlled ovarian hyperstimulation compared to WT mice. (b) Estradiol levels were higher after superovulation than in WT mice (Figure 8b). (n = 7, $^{*}P < 0.05$; $^{**}P < 0.01$).

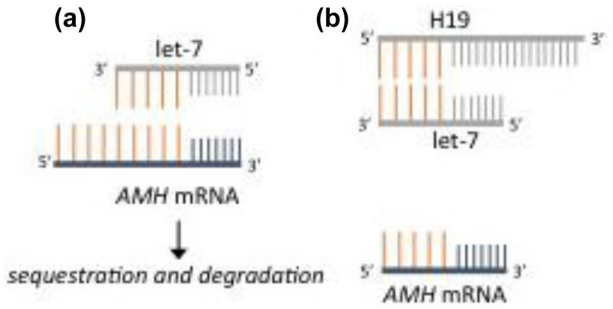

Figure 9. A proposed model for H19/let-7 mediated regulation of H19. (a) In the absence of H19, sequestration of let-7 does not occur and let-7 targets (including AMH) are degraded. (b) H19 sequesters let-7, thus sparing let-7 targets from degradation.

the regulation of follicular atresia is complex, involving endocrine factors such as FSH and LH, paracrine factors including fibroblast growth factor and endocrine growth factor, among many others [33], and the possible roles of H19 in the regulation of follicular development are still not well characterized. Thus, it may be that absence of H19 has additional effects on mediators of follicular atresia which are still poorly understood at this time.

We were surprised to observe that H19KO female mice, while subfertile in the setting of physiologic estrus cyclicity, demonstrate enhanced sensitivity to exogenous FSH with increased oocyte yield and estradiol levels after ovarian superovulation. AMHKO females are also subfertile, but not infertile, and in the absence of AMH, follicles are more sensitive to FSH, with higher numbers of proliferating granulosa cells found in follicles that express less AMH, and more pronounced stimulation of follicle growth in AMHKO females in the presence of high serum FSH concentrations compared to wild type females [34, 3]. Thus, these two mouse models appear to share many phenotypic similarities. While the H19KO mice does not exhibit complete lack of AMH, the decrease in AMH production seen in the H19KO mouse, and the similarity between the two phenotypes, supports our hypothesis that H19 may serve as a novel regulator of AMH.

One important and unresolved question concerns the pattern of H19 and let-7 expression in ovary. Ariel et al. [12] noted prominent expression of H19 in theca of antral follicles, and in granulosa cells of corpora lutea, in human ovarian sections from seven women. As AMH is expressed most highly in granulosa cells of small developing follicles, we might expect that H19 would also be expressed most highly during these same time points. However, it is important to note that the ovarian sections studied by Ariel et al. included women up to age 47 who were undergoing surgical removal of the ovaries due to various pathologies including ovarian tumors. Since it is well known that AMH expression declines with age and after chemotherapy for ovarian malignancies, the pattern observed by Ariel et al. may not be representative of a "typical" pattern of H19 expression in the ovary. In situ hybridization for miRNAs such as let-7 is technically challenging because conventional RNA or DNA probes display low affinity and low specificity for these small targets. Moreover, in our previous work, we demonstrated the functionality of H19/let-7 binding sites using reporter constructs and in vivo crosslinking assays [15]; however, let-7 levels themselves were not significantly altered in H19-expressing cells, suggested altered let-7 function without degradation of let-7 itself [15]. Additionally, H19 is highly expressed in skeletal and cardiac muscle and is detectable in plasma (Zhou et al. 2013 [35], Cancer Biomark, 17(2):187–194) and serum (Yang et al. 2016 [36], Cancer Epidemiol, 44:147–153), and circulating let-7 family members are well studied as biomarkers for various diseases. Thus, while the aforementioned studies suggest the presence of H19 in ovary, H19/let-7 mediated regulation of AMH is not necessarily dependent on this presence, but could also be due to serum or plasma levels of H19 and/or let-7. What is clear is that more work is needed to further clarify the spatiotemporal relationship of H19, let-7, and AMH in the mammalian ovary.

It has been suggested that AMH may have broadly important roles in health beyond its function in reproduction. AMH has been implicated in the pathogenesis of nonreproductive diseases, including cardiovascular disease (CVD). In a longitudinal Dutch cohort study of AMH trajectories in 3108 women, an association was observed between AMH levels and the rate of AMH decline and the incidence of coronary heart disease and CVD, with lower baseline circulating AMH levels and rapid rate of decline associated with higher risk. Notably, this result was independent of age, menopausal status, hormonal use, and metabolic and cardiovascular risk factors (Annelien C. de [37]). The authors postulated that the decline of circulating AMH levels could play a role in the pathophysiology of the increased cardiovascular risk observed at menopause. In individuals with premature ovarian insufficiency (the cause of which is frequently unknown, but can occur as a result of genetic causes such as Turner syndrome (a condition in which a female is partially or completely missing an X chromosome) or Fragile X (a disorder in which the CGG triplet repeat within the *FMR1* gene), autoimmune diseases such as autoimmune polyglandular syndrome, or treatment

with gonadotoxic therapies), the resultant early menopausal, hypoestrogenic state is strongly associated with higher CVD risk and mortality [38]. Predictably, in these situations, AMH can be used to assess the degree of follicular depletion, and early diminishment of AMH is predictive of early onset menopause as well as increased CVD risk ([39]; A.C. de [40]). This association may not be limited to females; in men, higher AMH levels were associated with an absence of CVD [41], and were inversely associated with aortic diameter [42]. Like the bone morphogenic protein family, which plays important roles in vascular homeostasis, AMH is also a member of the TGFβ superfamily ([43]; Annelien C. de [37]). Both H19 and Let-7 is highly expressed in the cardiovascular system and aberrant expression of both has been implicated in CVD states [44, 45]. Thus, although mechanistic insights are lacking, the possibility that H19, let-7, and AMH may be important determinants of adult CVD is an intriguing one and warrants further consideration.

In conclusion, we have identified AMH as a novel let-7 target, and H19 as a novel upstream regulator of AMH expression. Our results demonstrate that the inhibitory actions of AMH on follicle growth and gonadotropin responsiveness are regulated in part by H19 and let-7, marking this lncRNA/miRNA pair as important regulators of the establishment and maintenance of the primordial follicular pool. Future studies are in progress to further characterize the long-term fertility and ovarian reserve of the H19KO mouse.

Acknowledgment

The authors are grateful for H19 KO mice and technical support provided by Yingqun Huang, MD, PhD, Luisa Dandolo, PhD, and Stefan Muljo, PhD.

References

1. Blanchard MG, Josso N. Source of the Anti-müllerian hormone synthesized by the fetal testis: Müllerian-inhibiting activity of fetal bovine sertoli cells in tissue culture. *Pediatr Res* 1974; **8**:968–971.
2. Durlinger AL, Kramer P, Karels B, de Jong F, Uilenbroek JT, Grootegoed JA, Themmen AP. Control of primordial follicle recruitment by anti-Müllerian hormone in the mouse ovary. *Endocrinology* 1999; **140**:5789–5796.
3. Durlinger AL, Gruijters MJ, Kramer P, Karels B, Kumar TR, Matzuk MM, Rose UM, de Jong FH, Uilenbroek JT, Grootegoed JA, Themmen AP. Anti-Müllerian hormone attenuates the effects of FSH on follicle development in the mouse ovary. *Endocrinology* 2001; **142**:4891–4899.
4. Sacchi S, D'Ippolito G, Sena P, Marsella T, Tagliasacchi D, Maggi E, Argento C, Tirelli A, Giulini S, Marca AL. The anti-Müllerian hormone (AMH) acts as a gatekeeper of ovarian steroidogenesis inhibiting the granulosa cell response to both FSH and LH. *J Assist Reprod Genet* 2016; **33**:95–100.
5. Grynberg M, Pierre A, Rey R, Leclerc A, Arouche N, Hesters L, Catteau-Jonard S, Frydman R, Picard JY, Fanchin R, Veitia R, di Clemente N et al. Differential regulation of ovarian anti-Müllerian hormone (AMH) by estradiol through α- and β-estrogen receptors. *J Clin Endocrinol Metab* 2012; **97**:E1649–E1657.
6. Convissar S, Armouti M, Fierro M, Winston N, Scoccia H, Musa Zamah A, Stocco C. Regulation of AMH by oocyte-specific growth factors in human primary cumulus cells. *Reproduction* 2017; **154**:745–753.
7. Cech TR, Steitz JA. Review the noncoding RNA revolution — trashing old rules to forge new ones. *Cell* 2014; **157**:77–94.
8. Lei L, Jin S, Gonzalez G, Behringer RR, Woodruff TK. The regulatory role of Dicer in folliculogenesis in mice. *Mol Cell Endocrinol* 2010; **315**:63–73.
9. Hayes E, Kushnir V, Ma X, Biswas A, Prizant H, Gleicher N, Sen A. Intracellular mechanism of anti-Müllerian hormone (AMH) in regulation of follicular development. *Mol Cell Endocrinol* 2016; **433**:56–65.
10. Kimura AP, Yoneda R, Kurihara M, Mayama S, Matsubara S. A long noncoding RNA, lncRNA-Amhr2, plays a role in Amhr2 gene activation in mouse ovarian granulosa cells. *Endocrinology* 2017; **158**:4105–4121.
11. Rachmilewitz J, Goshen R, Ariel I, Schneider T, de Groot N, Hochberg A. Parental imprinting of the human H19 gene. *FEBS Lett* 1992; **309**:25–28.
12. Ariel I, Weinstein D, Voutilainen R, Schneider T, Lustig-Yariv O, De-Groot N, Hochberg A. The expression of the imprinted gene H19 in the human female reproductive organs. *Diagn Mol Pathol* 1997; **61**:17–25.
13. Khatib H, Schutzkus V. The expression profile of the H19 gene in cattle. *Mamm Genome* 2006; **17**:991–996.
14. Lagos-Quintana M. Identification of novel genes coding for small expressed RNAs. *Science* 2001; **294**:853–858.
15. Kallen AN, Zhou X, Xu J, Qiao C, Ma J, Yan L, Lu L, Liu C, Yi JS, Zhang H, Min W, Bennett AM et al. The imprinted H19 LncRNA antagonizes Let-7 microRNAs. *Mol Cell* 2013; **52**:101–112.
16. Men Y, Fan Y, Shen Y, Lu L, Kallen AN. The steroidogenic acute regulatory protein (StAR) is regulated by the H19/let-7 Axis. *Endocrinology* 2017; **158**:402–409.
17. Stocco DM, Selvaraj V. Yet another scenario in the regulation of the steroidogenic acute regulatory (STAR) protein gene. *Endocrinology* 2017; **158**:235–238.
18. Imig J, Brunschweiger A, Brümmer A, Guennewig B, Mittal N, Kishore S, Tsikrika P, Gerber AP, Zavolan M, Hall J. miR-CLIP capture of a miRNA targetome uncovers a lincRNA H19–miR-106a interaction. *Nat Chem Biol* 2015; **11**:107–114.
19. Li Z, Li Y, Li Y, Ren K, Li X, Han X, Wang J. Long non-coding RNA H19 promotes the proliferation and invasion of breast cancer through upregulating DNMT1 expression by sponging miR-152. *J Biochem Mol Toxicol* 2017; **31**:1–9.
20. Ou L, Wang D, Zhang H, Yu Q, Hua F. Decreased expression of MiR-138-5p by LncRNA H19 in cervical cancer promotes tumor proliferation. *Oncol Res* 2017. doi:10.3727/096504017X15017209042610.
21. Zhou W, Ye X-L, Xu J, Cao M-G, Fang Z-Y, Li L-Y, Guan G-H, Liu Q, Qian Y-H, Xie D. The lncRNA H19 mediates breast cancer cell plasticity during EMT and MET plasticity by differentially sponging miR-200b/c and let-7b. *Sci Signal* 2017; **10**:eaak9557.
22. Gabory A, Ripoche M-A, Digarcher AL, Watrin F, Ziyyat A, Forné T, Jammes H, Ainscough JF, Surani MA, Journot L, Dandolo L. H19 acts as a trans regulator of the imprinted gene network controlling growth in mice. *Development* 2009; **136**:3413–3421.
23. Caligioni CS. Assessing reproductive status/stages in mice. *Curr Protoc Neurosci* 2009; **48**:1–11.
24. Gay VL. Patterns of gonadotrophin secretion associated with ovulation. *Fed Proc* 1970; **29**:1880–1887.
25. Rehmsmeier M, Steffen P, Höchsmann M, Giegerich R, Ho M. Fast and effective prediction of microRNA /target duplexes. *Spring* 2004; **2003**:1507–1517.
26. Nishi Y, Yanase T, Mu Y et al. Establishment and characterization of a steroidogenic human granulosa-like tumor cell line, KGN, that expresses functional follicle-stimulating hormone receptor. *Endocrinology* 2001; **142**(1):437–445.
27. Dioguardi CC, Uslu B, Haynes M, Kurus M, Gul M, Miao DQ, De Santis L, Ferrari M, Bellone S, Santin A, Giulivi C, Hoffman G et al. Granulosa cell and oocyte mitochondrial abnormalities in a mouse model of fragile X primary ovarian insufficiency. *Mol Hum Reprod* 2016; **22**:384–396.
28. Uslu B, Dioguardi CC, Haynes M, Miao D-Q, Kurus M, Hoffman G, Johnson J. Quantifying growing versus non-growing ovarian follicles in the mouse. *J Ovarian Res* 2017; **10**:1.
29. Visser JA, Schipper I, Laven JS, Themmen AP. Anti-Müllerian hormone: an ovarian reserve marker in primary ovarian insufficiency. *Nat Rev Endocrinol* 2012; **8**:331–341.
30. Broer SL, Broekmans FJ, Laven JS, Fauser BC. Anti-Müllerian hormone: ovarian reserve testing and its potential clinical implications. *Hum Reprod Update* 2014; **20**:688–701.
31. Seifer DB, MacLaughlin DT, Christian BP, Feng B, Shelden RM. Early follicular serum müllerian-inhibiting substance levels are associated with ovarian response during assisted reproductive technology cycles. *Fertil Steril* 2002; **77**:468–471.

32. Weenen C, Laven JS, von Bergh AR, Cranfield M, Groome NP, Visser JA, Kramer P, Fauser BC, Themmen AP. Anti-Mullerian hormone expression pattern in the human ovary: potential implications for initial and cyclic follicle recruitment. *Mol Hum Reprod* 2004; **10**:77–83.
33. Markström E, Svensson EC, Shao R, Svanberg B, Billig H. Survival factors regulating ovarian apoptosis – dependence on follicle differentiation. *Reproduction* 2002; **123**:23–30.
34. Durlinger AL, Visser JA, Themmen AP. Regulation of ovarian function: the role of anti-Mullerian hormone. *Reproduction* 2002; **124**:601–609.
35. Zhou X, Yin JC, Dang Y, Ye F, Zhang G. Identification of the long noncoding RNA H19 in plasma as a novel biomarker for diagnosis of gastric cancer. *Sci Rep* 2015; **5**:1–10.
36. Yang Y, Ren JL, Sun L, Huang C, Xiao B, Wang T, Chen J, Zabel B, Ren P, Zhang J. The role of GPR1 signaling in mice corpus luteum. *J Endocrinol* 2016; **230**:55–65.
37. Kat ACde, Monique Verschuren W, Eijkemans MJ, Broekmans FJ, van der Schouw YT. Anti-Müllerian hormone trajectories are associated with cardiovascular disease in womenclinical perspective. *Circulation* 2017; **135**:556–565.
38. Committee opinion no. 605: primary ovarian insufficiency in adolescents and young women. *Obstet Gynecol* 2014; **20**:245–247. doi:10.1097/SPV.0000000000000112.
39. Guzel Y, Aba YA, Yakin K, Oktem O. Menstrual cycle characteristics of young females with occult primary ovarian insufficiency at initial diagnosis and one-year follow-up with serum amh level and antral follicle count. *PLoS One* 2017; **12**:e0188334.
40. de Kat AC, Verschuren WM, Eijkemans MJ, van der Schouw YT, Broekmans FJ. The association of low ovarian reserve with cardiovascular disease risk: a cross-sectional population-based study. *Hum Reprod* 2016; **31**:1866–1874.
41. Chong YH, Dennis NA, Connolly MJ, Teh R, Jones GT, van Rij AM, Farrand S, Campbell AJ, MLennan IS. Elderly men have low levels of anti-Müllerian hormone and inhibin B, but with high interpersonal variation: a cross-sectional study of the sertoli cell hormones in 615 community-dwelling men. *PLoS One* 2013; **8**:e70967.
42. Dennis NA, Jones GT, Chong YH, van Rij AM, McLennan IS. Serum anti-Mullerian hormone (AMH) levels correlate with infrarenal aortic diameter in healthy older men: is AMH a cardiovascular hormone? *J Endocrinol* 2013; **219**:13–20.
43. Visser JA, Themmen APN. Role of anti-Müllerian hormone and bone morphogenetic proteins in the regulation of FSH sensitivity. *Mol Cell Endocrinol* 2014; **382**:460–465.
44. Bao MH, Feng X, Zhang YW, Lou XY, Cheng Y, Zhou HH. Let-7 in cardiovascular diseases, heart development and cardiovascular differentiation from stem cells. *Int J Mol Sci* 2013; **14**:23086–23102.
45. Gomes CPC, Spencer H, Ford KL, Michel LYM, Baker AH, Emanueli C, Balligand JL, Devaux Y. The function and therapeutic potential of long non-coding RNAs in cardiovascular development and disease. *Mol Ther Nucleic Acids* 2017; **8**:494–507.